2 Citron, S. J., *Elements of Optimal Control*, Holt, Rinehart and Winston, 1969.
3 Rao, S. N., and Luus, R., "Evaluation and Improvement of Control Vector Iteration Procedures for Optimal Control," *The Canadian Journal of Chemical Engineering*, Vol. 50, pp. 777–784, 1972.
4 Luenberger, D. G., *Linear and Nonlinear Programming*, Addison Wesley, Reading, Mass., 1984.

An Alternate Geometric Perspective on MIMO Systems

M. L. Nagurka[1] and T. R. Kurfess[1]

An alternate graphical representation of linear, time-invariant, multi-input, multi-output (MIMO) system dynamics is proposed that is highly suited for exploring the influence of closed-loop system parameters. The development is based on the adjustment of a scalar forward gain multiplying a cascaded multivariable controller/plant embedded in an output feedback configuration. By tracking the closed-loop eigenvalues as explicit functions of gain, it is possible to visualize the multivariable root loci in a set of "gain plots" consisting of two graphs: (i) magnitude of system eigenvalues versus gain and (ii) argument (angle) of system eigenvalues versus gain. The gain plots offer an alternative perspective of the standard MIMO root locus plot by depicting unambiguously the polar coordinates of each eigenvalue in the complex plane. Two example problems demonstrate the utility of gain plots for interpreting closed-loop multivariable system behavior.

Introduction

Since their introduction, classical control tools have been popular for analysis and design of single-input, single-output (SISO) systems. These tools may be viewed as specialized versions of more general methods that are applicable to multi-input, multi-output (MIMO) systems. Although modern "state-space" control techniques (relying on dynamic models of internal structure) are generally promoted as the predominant tools for multivariable system analysis, the classical control extensions offer several advantages, including requiring only an input-output map and providing direct insight into stability, performance, and robustness of MIMO systems. The understanding generated by these graphically based methods for the analysis and design of MIMO systems is a prime motivator of this research.

An early graphical method for investigating the stability of linear, time-invariant (LTI) SISO systems was developed by Nyquist (1932) and is based on a polar plot of the loop transmission transfer function. The MIMO analog of the Nyquist diagram is the multivariable Nyquist diagram which is used in conjunction with the corresponding multivariable Nyquist criterion (Rosenbrock, 1974; Lehtomaki et al., 1981; Friedland, 1986). This criterion is complicated in the MIMO case because it is expressed in terms of the determinant of the return difference transfer function matrix ($[\mathbf{I} + \mathbf{G}(s)]$ where $\mathbf{G}(s)$ is the open-loop system transfer function matrix, rather than just $1 + g(s)$ for the SISO case where $g(s)$ is the system transfer function). Despite the complication, significant research has supported the MIMO Nyquist extension for assessment of multivariable system stability and robustness (MacFarlane and Postlethwaite, 1977).

The Bode plots (Bode, 1940) recast the information of the Nyquist diagram, with frequency extracted as an explicit parameter. The MIMO analog or extension of the classical Bode magnitude plot is the singular value Bode-type plot that shows maximum and minimum singular values of transfer function matrices as a function of frequency (Doyle and Stein, 1981). This generalized magnitude versus frequency plot is useful for analysis, providing performance insight in terms of command following, disturbance rejection, modeling error, [redacted], and sensor noise sensitivity, as well as for design, in terms of frequency shaping (Doyle and Stein, 1981; Safanov et al., 1981; Athans, 1982; Maciejowski, 1989).

Although promoted as an SISO tool, Evans root locus method (Evans, 1954) is also extendable to MIMO systems since it depicts the trajectories of closed-loop eigenvalues (of either SISO or MIMO systems) in a complex plane. As such, it provides insight into stability and performance of the closed-loop system. However, the generalization to multivariable root loci has not made as significant an impact as the MIMO versions of the classical frequency-domain tools for a number of reasons. First, in similarity to the multivariable Nyquist diagram and Bode plot, the MIMO root locus plot does not, in general, follow the straightforward sketching rules applicable to SISO systems. Second, part of the complication of the MIMO root locus relates to the fact that "multivariable root loci live on a Riemann surface. . . as compared with the single-input, single-output case where the root loci lie on a simple complex plane (a trivial, i.e., one sheeted, Riemann surface)" (Postlethwaite and MacFarlane, 1979). As a result, multivariable root loci tend to have confusing patterns when drawn in a single complex plane, since loci can be multi-valued functions of gain.

To aid the controls engineer in extracting more information from the multivariable Evans root locus plot, we propose a set of "gain plots" that provide a direct and unique window into the stability, performance, and robustness of LTI MIMO systems. A conceptual framework motivating the gain plots and a discussion of their applicability to SISO systems has been presented previously (Kurfess and Nagurka, 1991).

Multivariable Eigenvalue Description

Basic MIMO Concepts. A LTI MIMO plant can be represented in the standard state-space form as

$$\dot{\mathbf{x}}_p(t) = \mathbf{A}_p\mathbf{x}_p(t) + \mathbf{B}_p\mathbf{u}(t) \tag{1}$$

$$\mathbf{y}(t) = \mathbf{C}_p\mathbf{x}_p(t) + \mathbf{D}_p\mathbf{u}(t) \tag{2}$$

where state vector $\mathbf{x}_p$ is length n, input vector $\mathbf{u}$ is length m, and output vector $\mathbf{y}$ is length m. Matrices $\mathbf{A}_p$, $\mathbf{B}_p$, $\mathbf{C}_p$, and $\mathbf{D}_p$ are the system matrix, the control influence matrix, the output matrix, and the feed-forward matrix, respectively, of the plant with appropriate dimensions. The plant input-output dynamics are governed by the transfer function matrix, $\mathbf{G}_p(s)$,

$$\mathbf{G}_p(s) = \mathbf{C}_p[s\mathbf{I} - \mathbf{A}_p]^{-1}\mathbf{B}_p + \mathbf{D}_p \tag{3}$$

The system is embedded in the closed-loop configuration shown in Fig. 1, where the controller is a dynamic compensator, $k\mathbf{G}_c(s)$, implying that each error signal is scaled by the same constant gain k. The controller transfer function matrix can be expressed as

$$\mathbf{G}_c(s) = \mathbf{C}_c[s\mathbf{I} - \mathbf{A}_c]^{-1}\mathbf{B}_c + \mathbf{D}_c \tag{4}$$

[1]Department of Mechanical Engineering, Carnegie Mellon University, Pittsburgh, PA 15213.

Contributed by the Dynamic Systems and Control Division of THE AMERICAN SOCIETY OF MECHANICAL ENGINEERS. Manuscript received by the Dynamic Systems and Control Division April 2, 1991; revised manuscript received November 2, 1992. Associate Technical Editor: J. L. Stein.

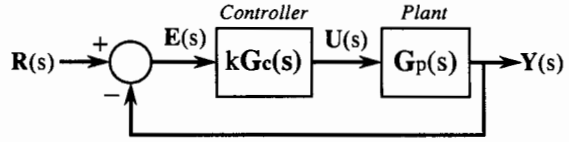

Fig. 1 MIMO closed-loop negative feedback configuration

where $\mathbf{A}_c$, $\mathbf{B}_c$, $\mathbf{C}_c$, and $\mathbf{D}_c$ are the controller matrices representing its internal structure, in similarity to Eqs. (1) and (2), with the controller input being the error, $\mathbf{e}(t)$, and the controller output being the plant input, $\mathbf{u}(t)$.

The closed-loop transfer function matrix, $\mathbf{G}^*(s)$, between the reference vector, $\mathbf{r}(t)$, of length m, and the output vector, $\mathbf{y}(t)$, is

$$\mathbf{G}^*(s) = [\mathbf{I} + k\mathbf{G}_p(s)\mathbf{G}_c(s)]^{-1}\mathbf{G}_p(s)\mathbf{G}_c(s)k \tag{5}$$

In the MIMO root locus plot, the migration of the eigenvalues of $\mathbf{G}^*(s)$ in the complex plane is graphed for $0 \le k < \infty$. (By equating the determinant of $[\mathbf{I} + k\mathbf{G}_p(s)\mathbf{G}_c(s)]$ to zero, the MIMO generalization of the SISO characteristic equation $1 + kg_p(s)g_c(s) = 0$ is obtained. The presence of the determinant is the major challenge in generalizing the SISO root locus sketching rules to MIMO systems and complicates the root locus plot.) The closed-loop system dynamics can alternatively be cast in state-space form in terms of state vector $\mathbf{x}(t) = [\mathbf{x}_p(t)\ \mathbf{x}_c(t)]^T$. The closed-loop system matrix then becomes

$$\mathbf{A}^* = \begin{bmatrix} \mathbf{A}_p - \mathbf{B}_p\mathbf{D}_c k\mathbf{M}^{-1}\mathbf{C}_p & \mathbf{B}_p\mathbf{C}_c - \mathbf{B}_p\mathbf{D}_c k\mathbf{M}^{-1}\mathbf{D}_p\mathbf{C}_c \\ -\mathbf{B}_c k\mathbf{M}^{-1}\mathbf{C}_p & \mathbf{A}_c - \mathbf{B}_c k\mathbf{M}^{-1}\mathbf{D}_p\mathbf{C}_c \end{bmatrix} \tag{6}$$

where $\mathbf{M} = [\mathbf{I} + \mathbf{D}_p\mathbf{D}_c k]$. The eigenvalues of the closed-loop system, $s = \lambda_i = \text{eig}(\mathbf{A}^*)$ $(i = 1, 2, \ldots, n)$, may be computed numerically from Eq. (6). In the examples, the loci of the eigenvalues are calculated as k is monotonically increased from zero.

High Gain Behavior. As the gain is swept from zero to infinity, the closed-loop eigenvalues trace out "root loci" in the complex plane. At zero gain, the poles of the closed-loop system are the open-loop eigenvalues. At infinite gain some of the eigenvalues approach finite transmission zeros, defined to be those values of s that satisfy the generalized eigenvalue problem. In the absence of pole/zero cancellation, the finite transmission zeros are the roots of the determinants of $\mathbf{G}_p(s)$ and $\mathbf{G}_c(s)$. Algorithms have been developed for efficient and accurate computation of transmission zeros (Davison and Wang, 1974; Laub and Moore, 1978; Westreich, 1991).

The eigenvalues can be considered as always migrating from the open-loop poles to their matching transmission zeros (Friedland, 1986). However, those eigenvalues that do not have matching zeros in the finite part of the s-plane are considered to have matching zeros at infinity. In the global SISO perspective, whenever there exists an excess of poles over zeros, the eigenvalues migrate toward infinity in a Butterworth configuration. If the excess of poles over zeros is greater than two for an SISO system the closed-loop eigenvalues must become unstable as $k \to \infty$. A single Butterworth configuration at high gain is generally not seen in the MIMO case; rather, multiple Butterworth configurations are generated. It can be shown that for a square system with m inputs, m outputs, and m or more eigenvalues migrating toward infinity, m high gain Butterworth patterns occur (on m different Riemann sheets) (Kwakernaak, 1976; Shaked,1978; Thompson et al., 1982). These patterns do not necessarily demonstrate criteria of the well known SISO Butterworth configurations (e.g., the angle criterion). The MIMO Butterworth patterns do, however, reveal the typical Butterworth magnitude characteristic demonstrated for SISO systems (Kurfess and Nagurka, 1992).

MIMO Gain Plots. Just as the Bode plots embellish the information of the Nyquist diagram by exposing frequency explicitly in a set of magnitude versus frequency and angle (phase) versus frequency plots, it follows that a pair of gain plots (Kurfess and Nagurka, 1991) can enhance the standard root locus plot. As the gain-domain analog of the frequency-domain Bode plots, the gain plots explicitly depict the eigenvalue magnitude versus gain in a magnitude gain plot, and the eigenvalue angle versus gain in an angle gain plot. In similarity to the Bode plots, the magnitude gain plot employs a log-log scale whereas the angle gain plot uses a semi-log scale (with the logarithms being base 10). Although gain is selected as the variable of interest in the gain plots, it should be noted that any scalar parameter may be used in the geometric analysis, leading to the more generic idea of parametric plots.

Gain plots can be drawn for both SISO and MIMO systems. In MIMO systems it is assumed that a single scalar gain amplifies all controller/plant inputs. For such systems, inspection of the magnitude and angle gain plots enables one to uniquely identify locus branches as a function of gain. As such, gain plots are a natural complement to multivariable root locus plots, where uncharacteristically confusing eigenvalue trajectories can result from being drawn in a single complex plane. Furthermore, it can be shown that the slopes of the lines in the gain plots are proportionally related to the root sensitivity function (Kurfess and Nagurka, 1992).

MIMO Examples

This section presents two multivariable examples. The first example introduces the concept of the gain plots and demonstrates the insight they offer by "unwrapping" the multivariable root locus and exposing unambiguous behavior. The second example highlights the power of the gain plots in revealing typical multivariable properties, such as high gain Butterworth patterns.

Example 1: Coupled MIMO Example. The forward loop dynamics of this example are given by the transfer function matrix

$$\mathbf{G}_p(s)\mathbf{G}_c(s) = \begin{bmatrix} \dfrac{(s-1)}{(s+1)(s+2)} & \dfrac{s}{(s+1)(s+2)} \\ \dfrac{-6}{(s+1)(s+2)} & \dfrac{(s-2)}{(s+1)(s+2)} \end{bmatrix} \tag{7}$$

(Equation (7) is used as an example by Postlethwaite and MacFarlane (1979) and later by Yagle (1981).) The MIMO root locus diagram, shown in Fig. 2, depicts two eigenvalue trajectories beginning at $s = -1$ and $s = -2$. The eigenvalue at $s = -2$ follows a trajectory along the negative real axis. The eigenvalue at $s = -1$ initially migrates to the right, proceeding to $s = 1/24 \approx 0.042$, and then reverses, moving back to the left of the imaginary axis. Both eigenvalues are always purely real. Notice that Fig. 2 does not follow the rules of the familiar SISO root locus, and is counter-intuitive.

The gain plots presented in Fig. 3(a, b) show that gain values in the range $1 \le k \le 2$ yield an unstable closed-loop system. The stable-unstable transitions are highlighted by a 180 deg jump as the eigenvalue passes through the origin. In contrast, the standard root locus plot is confusing, with two Riemann surfaces collapsed into a single complex plane. Since the root

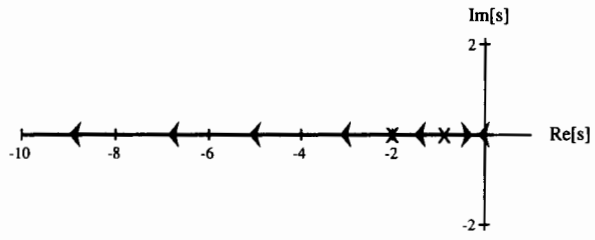

Fig. 2 Root locus plot of example 1

locus plot is drawn in two dimensions, branch points may be generated by more than one gain value and may not be uniquely presented. The gain plots, in contrast, display eigenvalue magnitude and angle information in an unambiguous and concise manner.

Example 2: Aircraft Vertical Plane Dynamics. The state space model (from Hung and MacFarlane (1982) and studied in detail by Maciejowski (1989)),

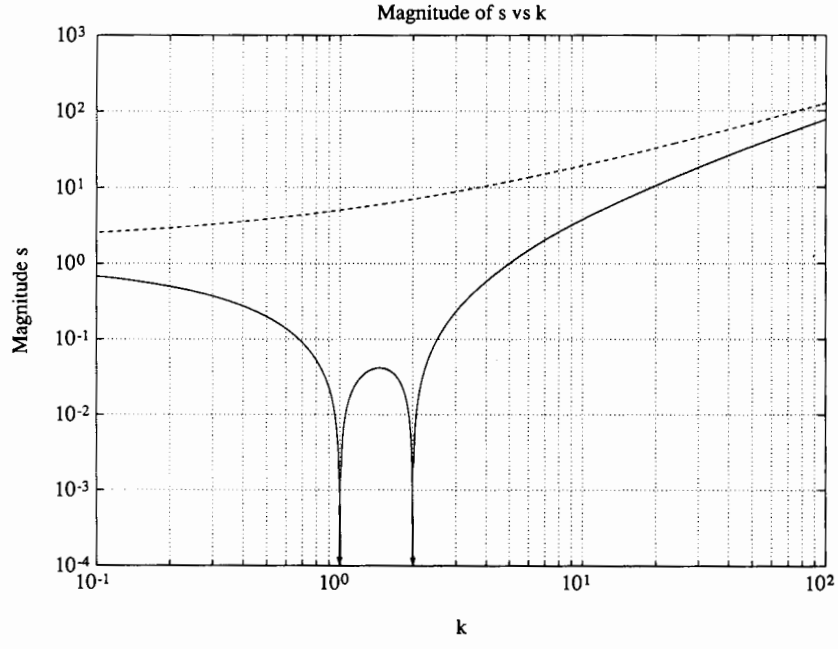

Fig. 3(*a*)

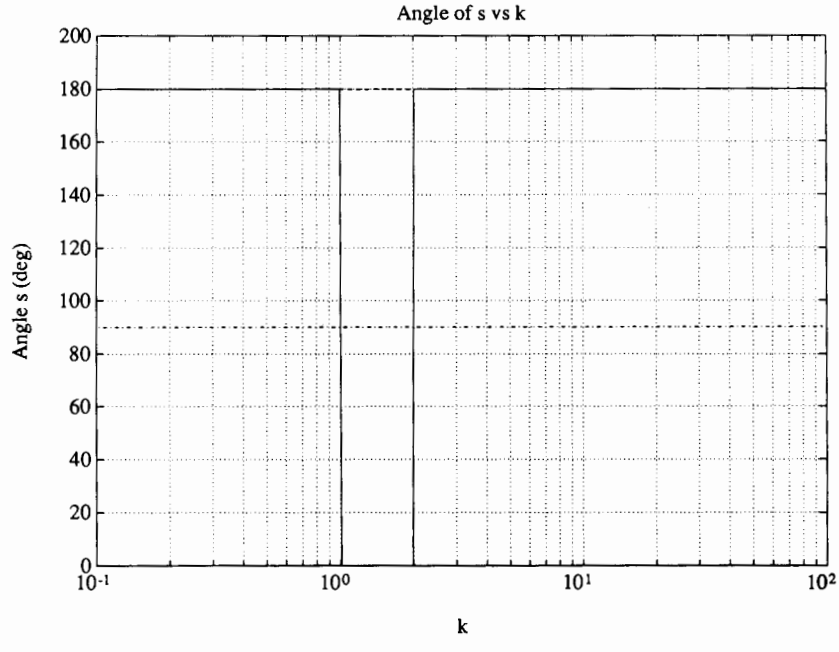

Fig. 3(*b*)

Fig. 3 (*a*) Magnitude and (*b*) angle gain plots of example 1

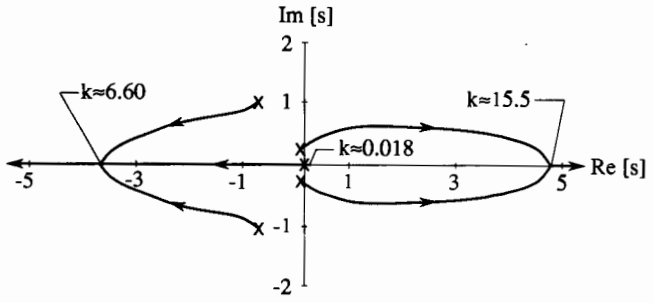

Fig. 4 Root locus plot of example 2

$$\dot{\mathbf{x}}_p = \begin{bmatrix} 0 & 0 & 1.132 & 0 & -1 \\ 0 & -0.054 & -0.171 & 0 & 0.071 \\ 0 & 0 & 0 & 1 & 0 \\ 0 & 0.049 & 0 & -0.856 & -1.013 \\ 0 & -0.291 & 0 & 1.053 & -0.686 \end{bmatrix} \mathbf{x}_p + \begin{bmatrix} 0 & 0 & 0 \\ -0.120 & 1 & 0 \\ 0 & 0 & 0 \\ 4.419 & 0 & -1.665 \\ 1.575 & 0 & -0.073 \end{bmatrix} \mathbf{u} \quad (8)$$

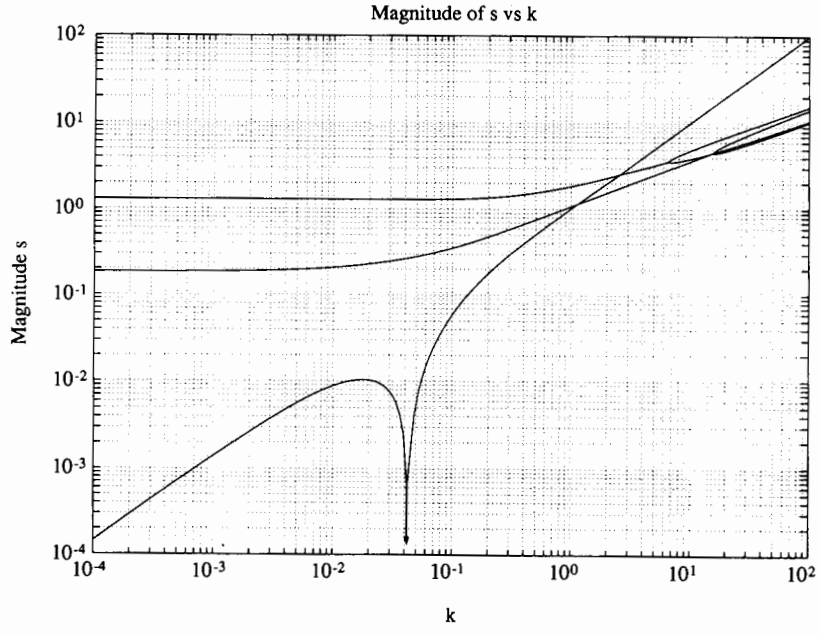

Fig. 5(*a*)

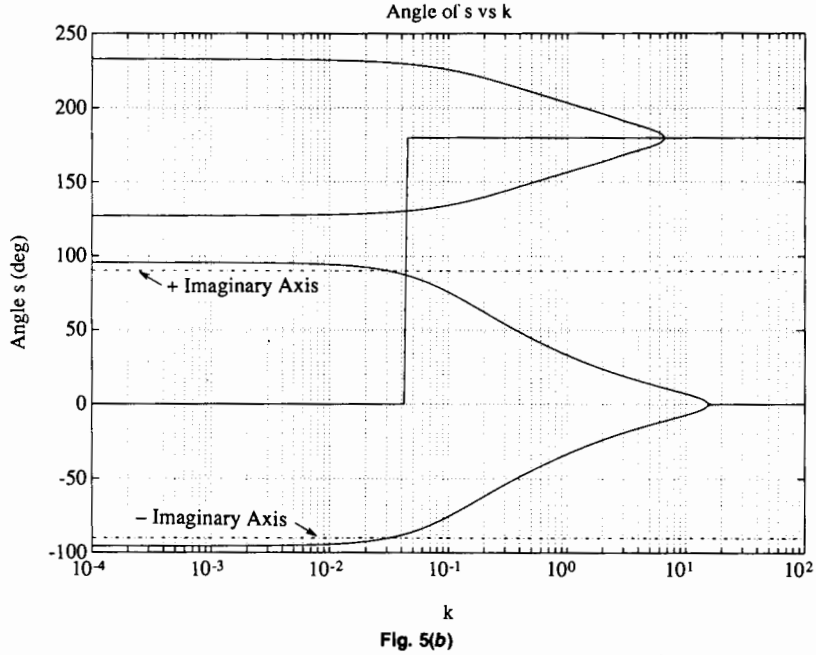

Fig. 5(*b*)

Fig. 5 (*a*) Magnitude and (*b*) angle gain plots of example 2

locus plot shown in Fig. 4. However, it is not clear if there exist gains for which all of the eigenvalues reside in the left-half plane, implying that the system is stable.

The gain plots for this system, appearing in Fig. 5(*a*, *b*), show that as the gain increases the eigenvalue at the origin initially migrates along the positive real axis (i.e., $\angle s = 0$ deg), indicating instability, until it reaches a maximum value of $s \approx 0.010$ at a gain $k \approx 0.018$. As the gain increases, this real eigenvalue reverses direction, crosses the imaginary axis at a gain $k \approx 0.043$, and continues to move along the negative real axis (i.e., $\angle s = 180$ deg). However, at $k \approx 0.043$ one pair of complex conjugate eigenvalues has already moved into the right-half plane (crossing the imaginary axis at the slightly lower gain of $k \approx 0.031$), as shown in the angle gain plot of Fig. 5(*b*). In summary, the gain plots provide an unambiguous means by which stability questions can be answered by inspection. In this case, the system is unstable for all gains.

The gain plots highlight several other important features. and then proceed toward $\pm\infty$. Complex conjugate eigenvalues are shown as symmetric lines about either the 180 or 0 deg line with equal magnitudes. Purely real eigenvalues possess equal angles (180 or 0 deg) but distinct magnitudes. This behavior is demonstrated in Fig. 5(*a*, *b*), from which the gains at the breakpoints may be determined directly.

The rates at which the eigenvalues increase toward infinite magnitude is seen in the magnitude gain plot of Fig. 5(*a*). The single eigenvalue that begins at the origin proceeds toward infinity (along the negative real axis) at a rate proportional to k as evident by the high gain magnitude gain plot slope of unity. This slope is characteristic of a first order Butterworth pattern. The two complex conjugate eigenvalue pairs proceed toward infinity at a rate proportional to $k^{1/2}$ (shown as a high gain magnitude gain plot slope of 1/2), indicative of a second order Butterworth pattern (Kurfess and Nagurka, 1992).

From Fig. 5(*a*), the two complex conjugate eigenvalue pairs at high gains have slope values of 1/2. As $k \to \infty$, this group of four parallel lines separates into two colinear sets. An interesting feature is that the two identical lines are comprised of an eigenvalue magnitude from each of the original complex conjugate pairs. This phenomenon is not apparent from the MIMO root locus, although it must occur due to the location of the centers of gravity for the two second order Butterworth patterns. Each set of colinear trajectories represents a Butterworth configuration.

Conclusions

In typical MIMO root locus plots trajectories may be camouflaged as branches may overlap. Gain plots are promoted as a means to "untangle" MIMO eigenvalue trajectories. The major enhancement is the visualization of eigenvalue trajectories as an explicit function of gain, assumed here to be the same static gain applied to all error signals.

The perspective presented in this note is intended to complement the multivariable root locus plot in much the same way that singular value frequency plots are an alternate and extended presentation of the multivariable Nyquist diagram. Their use in conjunction with the multivariable root locus provides a valuable geometric perspective on multivariable system behavior.

Acknowledgment

The authors wish to thank Mr. Ssu-Kuei Wang for his help, and for his earnest enthusiasm of gain plots for studying multivariable and optimal systems.

References

Amplifier Design," *Bell System Technical Journal*, Vol. 19, pp. 421–454.

Davison, E. J., and Wang, S. H., 1974, "Properties and Calculation of Transmission Zeros of Linear Multivariable Systems," *Automatica*, Vol. 10, pp. 643–658.

Doyle, J. C., and Stein, G., 1979, "Multivariable Feedback Design: Concepts for a Classical/Modern Synthesis," *IEEE Transactions on Automatic Control*, Vol. AC-26, pp. 4–16.

Evans, W. R., 1954, *Control System Dynamics*, McGraw-Hill, New York.

Friedland, B., 1986, *Control System Design*, McGraw-Hill, New York.

Hung, Y. S.,and MacFarlane, A. G. J., 1982, *Multivariable Feedback: A Quasi-Classical Approach*, Lecture Notes in Control and Information Sciences, Vol. 40, Springer-Verlag, Berlin.

Kurfess, T. R., and Nagurka, M. L., 1991, "A New Visualization of the Evans Root Locus: Gain Plots," *Robust Control of Mechanical Systems: Theory and Applications*, DSC-Vol.27, ASME Winter Annual Meeting, Atlanta, GA, pp. 1–8.

Kurfess, T. R., and Nagurka, M. L., 1993, "Foundations of Classical Control Theory with Reference to Eigenvalue Geometry," *Journal of The Franklin Institute*, Vol. 330, No. 2, pp. 213–227.

Kwakernaak, H., 1976, "Asymptotic Root Loci of Multivariable Linear Optimal Regulators," *IEEE Transactions on Automatic Control*, Vol. AC-21, No. 3, pp. 378–382.

Laub, A. J., and Moore, B. C., 1978, "Calculation of Transmission Zeros Using QZ Techniques," *Automatica*, Vol. 14, No. 6, pp. 557–566.

Lehtomaki, N. A., Sandell, N. R., Jr., and Athans, M., 1981, "Robustness Results in Linear-Quadratic Gaussian Based Multivariable Control Designs," *IEEE Transactions on Automatic Control*, Vol. AC-26, No. 1, pp. 75–93.

Maciejowski, J. M., 1989, *Multivariable Feedback Design*, Addison-Wesley Publishing Co., Reading, MA.

MacFarlane, A.G. J., and Postlethwaite, I., 1977, "The Generalized Nyquist Stability Criterion and Multivariable Root Loci," *International Journal of Control*, Vol. 25, pp. 81–127.

Nyquist, H., 1932, "Regeneration Theory," *Bell System Technical Journal*, Vol. 11, pp. 126–147.

Postlethwaite, I., and MacFarlane, A. G. J., 1979, *A Complex Variable Approach to the Analysis of Linear Multivariable Feedback Systems*, Lecture Notes in Control and Information Science, Springer-Verlag, New York, NY.

Rosenbrock, H. H., 1974, *Computer-Aided Control System Design*, Academic Press, London.

Safanov, M. G., Laub, A. J., and Hartmann, G. L., 1981, "Feedback Properties of Multivariable Systems: The Role and Use of the Return Difference Matrix," *IEEE Transactions on Automatic Control*, Vol. AC-26, No. 1, pp. 47–65.

Shaked, U., 1978, "The Asymptotic Behavior of Multivariable Optimal Regulators," *IEEE Transactions on Automatic Control*, Vol. AC-23, No. 3, pp. 425–430.

Thompson, P. M., Stein, G., and Laub, A. J., 1982, "Angles of Multivariable Root Loci," *IEEE Transactions on Automatic Control*, Vol. AC-27, No. 6, pp. 1241-1243.

Westreich, D., 1991, "Computing Transfer Function Zeros of a State Space System," *International Journal of Control*, Vol. 53, No. 2, pp. 477-493.

Yagle, A. E.,1981, *Properties of Multivariable Root Loci*, S. M. thesis, Department of Electrical Engineering and Computer Science, Massachusetts Institute of Technology, Cambridge, MA.

A New Plug-In Adaptive Controller for Rejection of Periodic Disturbances

Jwusheng Hu[1] and Masayoshi Tomizuka[2]

In this paper, an adaptive digital algorithm for rejecting periodic disturbances is proposed. Modified from the adaptive tracking controller [4], the controller is constructed in a "plug-in" manner, i.e., it can be added to an existed feedback control system without altering the original closed-loop configuration. It is shown that the controller can reject disturbances at selected frequencies independently. Furthermore, since the controller only deals with phase and gain of the error signal, no structural information about the plant is required. The controller is implemented on a disk drive system for track following. The result shows that by rejecting the disturbance up to four times of its fundamental frequency, the tracking error is reduced substantially.

1 Introduction

To reject periodic distrubances in linear time invariant systems, repetitive controllers [2, 3, 6, 10] proved to be efficient and effective. While many applications [7, 9, 11, 12] about repetitive control systems have been studied, certain issues such as unmodeled dynamics must be carefully handled to prevent instability. In view of the discrete time "internal model" [10], the repetitive controller generates control signals consisting of N frequencies, where N is the period. It has been shown in [4] that by treating each frequency separately, the structural information about the plant is not required. However, controllers presented in [4] are designed to fulfill the tracking performance specification. For disturbance rejection, it is not possible to use those controllers since there is no measurement of disturbances. In this paper, an alternative implementation of the adaptive tracking controller is presented. The idea of this particular controller structure is adopted from the prototype plug-in repetitive controller developed in [1]. In [1], the plug-in module can be added to any existing control loop to perform repetitive tracking or disturbance rejection. For example, it can be used to enhance the performance of a system under analog servo loop without replacing electrical elements. Another feature is that turning on/off the plug module will not affect the original controller structure. These appealing advantages make the plug-in type controller useful in applications such as disk drive control system.

An implementation example of the plug-in type adaptive controller on a disk drive system is presented in this paper. Due to imperfect disk shape, the read/write head of the drive has to follow tracks which are not perfectly circular [8]. Hence, compensators designed for regulation cannot achieve asymptotic tracking of the actual track. The offset is periodic with frequencies appearing at integer-multiple of the fundamental harmonic (rotating speed of the disk). Both internal and external based repetitive controllers have been implemented on this system [9] successfully. However, the performance of these algorithms depends on the accuracy of a system model. At the mass-production stage, fine tuning of the controller may still be required to accommodate differences among products. For example, unless the q-filter is added, the repetitive controller is very sensitive to unstructured model uncertainty. Conversely, the adaptive controller is capable of adjusting its parameters according to the system's frequency response. It is robust as long as the frequency response is not drastically changed. Also, after going through every track, which can be done during the manufacturing stage, the eccentricity of each track can be memorized and used as an initial guess so that a fast convergence can be achieved.

In order to keep up with the disk speed (60 Hz), the algorithm is implemented by fixed point calculations. Furthermore, the parallel implementation ability of the proposed controller is demonstrated by running the control algorithm in two computers simultaneously.

2 The Plug-In Module

In this section, we consider the case of a continuous plant under a nominal feedback compensation. Let $G_p(s)$ be the plant and $G_c(s)$ be the feedback controller. The structure of the overall control system is depicted in Fig. 1. In Fig. 1, d_1 can be an unknown reference signal and d_2 is the disturbance at the input side of the system. The discrete dynamic equation of Fig. 1 is

$$e(k) = G_s(z^{-1})u(k) + G_1(z^{-1})d_1(k) + G_2(z^{-1})d_2(k) \quad (1)$$

where $G_s(z^{-1})$, $G_1(z^{-1})$, and $G_2(z^{-1})$ are z-transforms of the closed-loop transfer functions. It is assumed that the nominal compensated system is stable. Furthermore, both $d_1(k)$ and $d_2(k)$ are periodic with the same period N. Since the plug-in module does not change the closed-loop transfer function of the nominal system, Eq. (1) can be rewritten as

$$e(k) = G_s(z^{-1})u(k) + w(k) \quad (2)$$

where $w(k)$, ignoring its transient, is also periodic with period N. So it can be represented as

$$w(k) = \sum_{n=0}^{N-1} \hat{w}_n e^{j\omega_n k}, \ \omega_n = \frac{2\pi n}{N} \quad (3)$$

As a result, if the input is designed to be

$$u(k) = -\sum_{n=0}^{N-1} (A_n + jB_n)\hat{w}_n e^{j\omega_n k}$$

where

$$A_n + jB_n = 1/G_s(e^{j\omega_n}),$$

the error $e(k)$ will reach zero asymptotically provided that $G_s(e^{j\omega_n}) \neq 0$. These formulations are essentially the same as those in [4] except that in [4], the reference signal is known while in Eq. (3), $\hat{w}_n$'s are unknown in advance. However, the theories developed in [4] can still be applied here with some modifications. Let $w(k)$ consist of only one frequency, i.e.,

$$w(k) = \hat{w}_n e^{j\omega_n k} + \overline{\hat{w}}_n e^{-j\omega_n k}$$

Since $w(k)$ is unknown, the input is then designed as

[1]Assistant Professor, Department of Mechanical Engineering, Wayne State University, Detroit, MI 48202.

[2]Professor, Department of Mechanical Engineering, University of California, Berkeley, CA 94720.

Contributed by the Dynamic Systems and Control Division of THE AMERICAN SOCIETY OF MECHANICAL ENGINEERS. Manuscript received by the Dynamics Systems and Control Division April 3, 1992; revised manuscript received July 1, 1992. Associate Technical Editor: S. Jayasuriya.

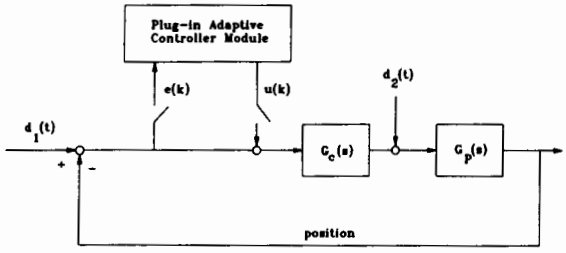

Fig. 1 Structure of the plug-in adaptive controller

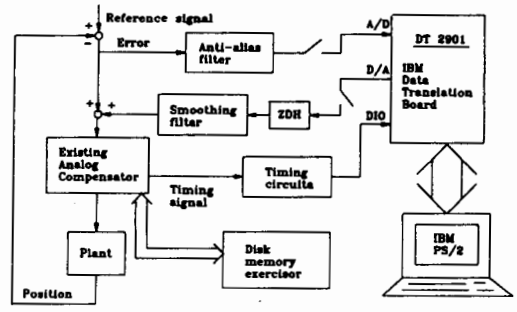

Fig. 2 Configuration of the disk drive control system

$$u(k) = \hat{C}_n \frac{1}{2}(e^{j\omega_n k} + e^{-j\omega_n k}) - \hat{D}_n \frac{j}{2}(e^{j\omega_n k} - e^{-j\omega_n k})$$

$$= \hat{C}_n \cos\omega_n k + \hat{D}_n \sin\omega_n k$$

$$= \hat{\theta}_n^T \phi_n(k) \tag{4}$$

where

$$\hat{\theta}_n = (\hat{C}_n \hat{D}_n)^T,\ \phi_n(k) = (\cos\omega_n k \sin\omega_n k)^T$$

and $\hat{C}_n$ and $\hat{D}_n$ are estimated real part and imaginary part of $-(A_n + jB_n)\hat{w}_n$. The error signal which drives the LMS adaptive algorithms is chosen as

$$e_n(k) = f_n(z^{-1}) \frac{(1-z^{-N})}{N} e(k) \tag{5}$$

where

$$f_n(z^{-1}) = \frac{(2 - 2\cos(\omega_n)z^{-1})}{1 - 2\cos(\omega_n)z^{-1} + z^{-2}}$$

To calculate $e_n(k)$, one can either implement Eq. (5) with the corresponding filter arrangement, or expand Eq. (5) into its DFT (Digital Fourier Transform) equivalence. The DFT scheme is essentially a moving average filter which may require more computing time than Eq. (5).

The LMS algorithm, driven by $e_n(k)$, is

$$\hat{\theta}_n(k+1) = \hat{\theta}_n(k) + \mu_n e_n(k)\phi_n(k) \tag{6}$$

To prove the stability, the error dynamic are derived as

$$\tilde{\theta}_n(k+1) = \tilde{\theta}_n(k) + \mu_n \phi_n(k)\left[\frac{(1-z^{-N})}{N} f_n(z^{-1}) G_s(z^{-1}) \tilde{\theta}_n^T(k)\phi_n(k)\right] + \mu_n E_n(k)\phi_n(k) \tag{7}$$

where

$$\tilde{\theta}_n(k) = \hat{\theta}_n(k) - \theta_n,\ \theta_n = (C_n D_n)^T$$

$$A_n = \Re[1/G_s(e^{j\omega_n})],\ B_n = \Im[1/G_s(e^{j\omega_n})]$$

and

$$E_n(k) = \frac{(1-z^{-N})}{N} f_n(z^{-1})[G_s(z^{-1})\theta_n^T \phi_n(k) + w(k)]$$

The following theorem states the condition on μ_n to guarantee convergence of $\tilde{\theta}_n(k)$.

Theorem 1. $\tilde{\theta}_n(k)$, governed by Eq. (7), converges to zero if the following conditions are satisfied:

$$\mu_n < 0 \text{ if } -\frac{\pi}{2} \le \text{Arg}(G_s(e^{j\omega_n})) \le \frac{\pi}{2}$$

$$\mu_n > 0 \text{ if } \frac{\pi}{2} < \text{Arg}(G_s(e^{j\omega_n})) < \frac{3\pi}{2}$$

and

$$\sup_{\Omega \in K} \frac{\mu_n[(\cos\omega_n - \cos\Omega)^2 + \sin^2\Omega]}{2N(\cos\omega_n - \cos\Omega)^2} \Re(G(e^{j\Omega})) < 1$$

where

$$K = \{\Omega \mid (1 - \cos(N\Omega))\Im(G_s(e^{j\Omega})) + \Re(G_s(e^{j\Omega}))\sin(N\Omega) = 0,\ \Omega \in [0, \pi]\}$$

[Proof]: referred to [4].

Notice that in this theorem, the magnitude of $\hat{w}_n$ does not appear in the stability condition since it is lumped into the parameter vector $\tilde{\theta}_n$. The derivations for multiple frequencies are the same as described in [4] and they are omitted.

3 The Disk Drive Experiment

The plug-in adaptive controller is implemented on a magnetic disk drive system. The goal of this controller is to eliminate the periodic errors induced by imperfect shape of the disk.

3.1 System Description. The disk used is a Fujitsu model M2333K which is an 8 in. rigid disk whose data storage capacity is 335 megabytes. Detailed technical information can be found in [5]. The angular speed of the disks is 60 Hz and is assumed to be constant.

The interface circuits are built using discrete components. They consist of a first order anti-aliasing filter, a first order low-pass filter to smooth the output of the zeroth order holder, a summing junction, and a timer circuit to extend the duration the index pulse used to monitor the rotational position of the disk. The anti-alias filter is adjusted to have a -3 db gain at the frequency of 600 Hz, which corresponds to slightly less than half the sampling frequency. Also, the DC gain is adjusted to 15 to use the full resolution of the A/D converter. The time constant of the smoothing filter is set to approximately 82 μs, roughly eight times less than the sampling time.

The computer used in this experiment is an IBM PS/2 model 80 with an Intel 80386 processor and 80387 math co-processor. The on-board clock of the machine is 25 MHz. I/O functions are done by using the IBM data translation board DT-2901. Fig. 2 depicts the overall configuration of the control system.

3.2 Simulation. The discrete time transfer function, from $u(k)$ to $e(k)$ (Fig. 2), associated with 28 samples per revolution is identified as

$$G_s(z^{-1}) = \frac{15z^{-2}(-0.6553 - 0.1140z^{-1})}{1 - 0.4985z^{-1} + 0.1587z^{-2}} \tag{8}$$

The disturbance used for simulation consists of a deterministic signal with four distinct frequencies, i.e., 60, 120, 180, and 240 Hz, and a random signal (Fig. 3). Figure 4 shows its average spectrum for 40 trials. Figure 5 depicts the error spectrum by using the fixed-point calculation. An interesting point is that the parameters adapted do not converge to constants as shown in Fig. 6. Instead, they fluctuate around constant levels. One reason is that the FSF (Frequency Sampling Filter) does not completely block the signals whose frequencies are not integer-multiple of the fundamental frequency. At steady state, this